Tectonophysics, 113 (1985) 271–282
Elsevier Science Publishers B.V., Amsterdam – Printed in The Netherlands

A BODY-WAVE ANALYSIS OF THE 1966 GISBORNE, NEW ZEALAND, EARTHQUAKE

TERRY H. WEBB *, S.G. WESNOUSKY and DONALD V. HELMBERGER

Seismological Laboratory, California Institute of Technology, Pasadena, CA 91125 (U.S.A.)

(Received September 10, 1984; revised version accepted October 1, 1984)

ABSTRACT

Webb, T.H., Wesnousky, S.G. and Helmberger, D.V., 1985. A body-wave analysis of the 1966 Gisborne, New Zealand, earthquake. *Tectonophysics*, 113: 271–282.

The $M_L = 6.2$ Gisborne earthquake of March 4, 1966 occurred along the East Coast of the North Island, New Zealand. Modeling of P and S body waves shows that the focal mechanism of this event is consistent with northwestward thrusting of the Pacific Plate beneath the North Island ($\varphi = 249°$, $\delta = 25°$ and $\lambda = 131°$). The focal depth is constrained to 18 km, significantly less than the values of 25–30 km computed from local network data. Estimates of the scalar moment, source duration and stress-drop for the event are 4×10^{24} dyne-cm, 2–3 s, and 20–120 bar, respectively. Cross-correlation errors of synthetic to observed waveforms were computed for all possible *P* and *T* axis locations and slip vector orientations and contoured on a projection of the focal sphere. The error contour at which the synthetic waveforms distinctly diverged from the observed waveforms was established by eye. The procedure shows that the analysis of long-period body waves, at least in this case, provides much better constraint on focal mechanism orientation than does first motion data alone.

INTRODUCTION

The North Island of New Zealand is located along the eastern edge of the Indian Plate and is bounded to the east by the Pacific Plate (Fig. 1). The location of the Hikurangi Trench and a well-developed Wadati–Benioff zone extending northwestward beneath the North Island are consistent with plate tectonic models indicating ongoing subduction of the Pacific Plate (Fig. 1). Although a number of large earthquakes has been recorded along this plate boundary during historic time (e.g. the 1931 Napier earthquake of magnitude 7.9), no events of magnitude greater than about 6.2 have occurred since the establishment of the WWSSN. As a result, constraints on the tectonic deformation of the region have been primarily supplied in two ways. First, by microearthquake studies of specific regions using portable

* Present address: Geophysics Division, D.S.I.R., P.O. Box 1320, Wellington, New Zealand.

0040-1951/85/$03.30

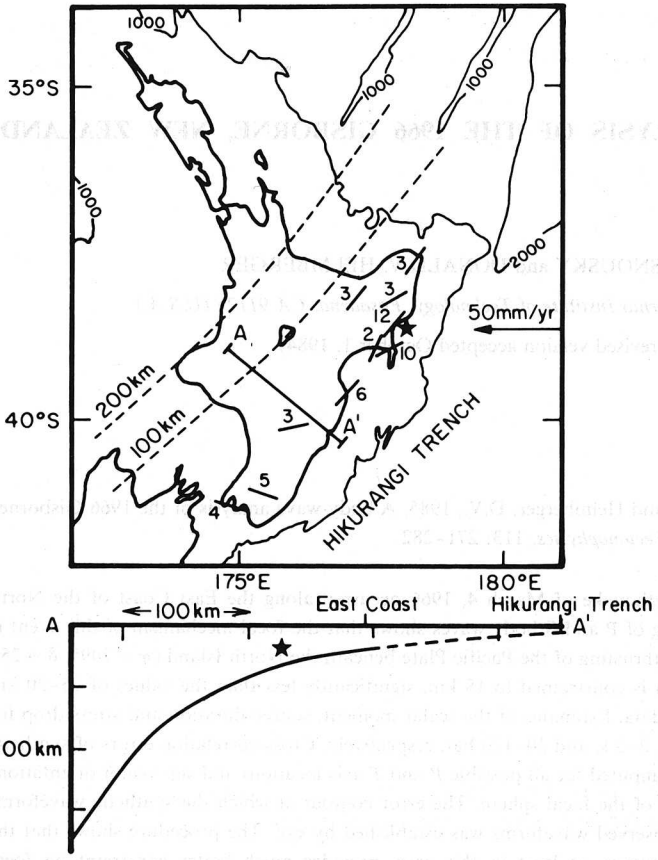

Fig. 1. Map of the North Island of New Zealand (adapted from Walcott, 1978) with 1000 and 2000 fathom bathymetry (1 fathom = 1.8 m), relative plate motion, and contours of deep earthquake locations from Adams and Ware (1977). The epicenter of the Gisborne earthquake is marked with a star. Solid bars show directions of principal axes of compression in units of 10^{-7}/yr for the period 1931 to 1970 from Walcott (1978). The cross-section shows the position of the upper surface of the subducted Pacific Plate inferred from microearthquake data by Reyners (1980) as well as the Gisborne event 200 km to the northeast.

instruments, and secondly, by short-period P-wave first motion mechanisms of moderate sized earthquakes recorded on the New Zealand seismograph network, which is really too sparse to provide reliable constraints on focal mechanisms. While these data have increased our knowledge of the regional tectonics, it is important to reliably establish the mechanism of the largest events along the plate boundary since they accommodate the major portion of the seismic deformation that is occurring.

It is thus the purpose of this paper to examine whether analysis of teleseismic P and S body waves can provide a better constraint on the focal mechanisms of moderate sized earthquakes along the East Coast of the North Island. Toward this

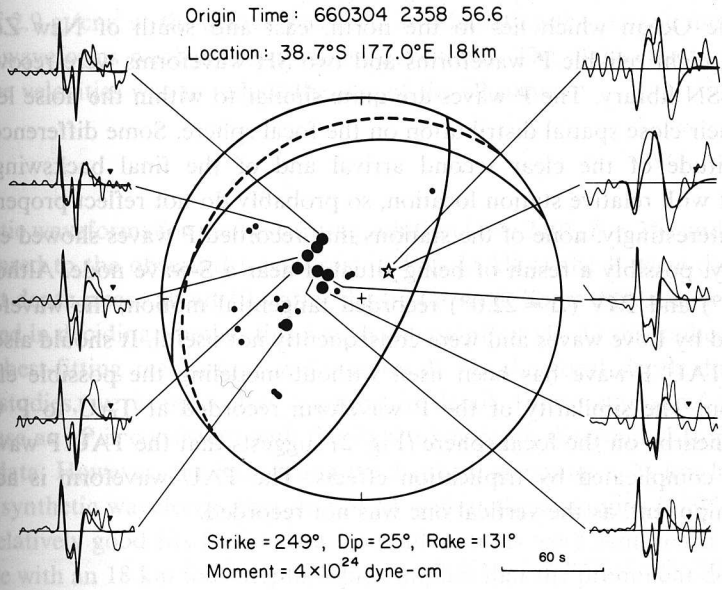

Fig. 2. Preferred mechanism for the Gisborne earthquake. Large circles indicate locations of the stations used in body-wave modeling, on an equal-area projection of the lower focal hemisphere. Small circles are stations for which short-period first motion data was available. The star marks the location of stations GSC and PAS at which SH waves were recorded. The dashed curve is the projection of the inferred subducted Pacific Plate under the North Island of New Zealand. For each station the data (thin lines) and synthetics (thick lines) for the best-fitting mechanism are shown. The small triangles shown above each waveform mark the point up to which cross-correlations were performed. A_d is the maximum zero to peak amplitude for the data and A_s that for the synthetic waveforms for a moment of 4×10^{24} dyne-cm.

end we have chosen to study the Gisborne earthquake of March 4, 1966.

The Gisborne earthquake was first studied by Hamilton (1969), who located the event at 38.5°S and 177.9°E (Fig. 1), and determined a local magnitude of 6.2. Johnson and Molnar (1972) examined regional and teleseismic first motion data and found a mechanism consistent with northwest thrusting, although they describe it as "not well determined". Observation of available first motion data (Fig. 2) and a plot of possible mechanisms that satisfy the data show this indeed to be the case. Recent reanalysis of the New Zealand network data does, however, show the depth of the earthquake to be well-constrained at 25–30 km (E.G.C. Smith, pers. commun., 1984).

TELESEISMIC DATA

The WWSSN stations that recorded P and S waves for the Gisborne earthquake are shown in Fig. 2. The azimuthal distribution of stations recording the event is poor, primarily due to the relatively small size of the event and the wide expanse of

the Pacific Ocean which lies to the north, east and south of New Zealand. In summary, eight reliable P waveforms and two SH waveforms were recovered from the WWSSN library. The P waves are quite similar to within the noise level, which reflects their close spatial distribution on the focal sphere. Some differences, such as the amplitude of the clear second arrival and of the final backswing, are not consistent with relative station location, so probably do not reflect properties of the source. Interestingly, none of the stations that recorded P waves showed evidence of SH energy, possibly a result of being situated near a S-wave node. Although TAU ($\Delta = 23.5°$) and RIV ($\Delta = 22.0°$) recorded tangential motion, the waveforms were dominated by Love waves and were consequently not useful. It should also be noted that the TAU P-wave has been used without modeling the possible effects of a triplication. The similarity of the P waveform recorded at TAU to P waveforms recorded nearby on the focal sphere (Fig. 2) suggests that the TAU P waveform has not been complicated by triplication effects. The TAU waveform is actually the radial component, as the vertical one was not recorded.

METHOD

Synthetic seismograms were produced following the method of Langston and Helmberger (1975). These were cross-correlated with the observed waveforms following the procedure proposed by Mellman et al. (1975). Since the data are quite sparse, an inversion procedure was not followed as it would be poorly conditioned. Instead, weighted errors derived from the cross-correlations were calculated for 10° steps in strike and rake, and 5° steps in dip. The resulting error maps were used to locate mechanisms producing synthetic waveforms that matched the data. This proved to be an efficient procedure since it was only necessary to perform the cross-correlations once for each of the three fundamental faults described by Langston and Helmberger (1975). Weights for individual stations were assigned according to signal-to-noise ratio and position on the focal sphere; all P waves except at TAU had a combined weight of 2, while the TAU P-wave, GSC and PAS SH waves each had a weight of 1.

The four remaining parameters controlling the shape of the synthetics are source time function, focal depth, attenuation and velocity model. The source time function was assumed to be a trapezoid (Langston and Helmberger, 1975) and was fit by forward modeling. The focal depth from local network data was used as a starting value. Since the time delay for the depth phases is reasonably large compared with the source duration, the depth phases are easily observed in the data. The usual values of 1.0 and 4.0 s were used for t^* in Futterman's (1962) attenuation operator for P and S waves respectively. Surface velocities for P and S waves of 3.5 and 2.0 km/s respectively, and a density of 2.6 g/cm^3 were used in calculating surface reflection coefficients for the depth phases. Respective velocities of 6.2 and 3.5 km/s for P and S waves were used in calculating take-off angles from the source, and a

density of 2.9 g/cm^3 at the source was used in calculating the seismic moment. The synthetic waveforms were not very model dependent. The main effect of lowering the surface velocities was to reduce the size of the sP phase.

RESULTS

Synthetic waveforms for the best-fitting solution ($\varphi = 249°$, $\delta = 25°$ and $\lambda = 131°$) are compared to the observed waveforms in Fig. 2. All of the P-wave data show a prominent depth phase about 10 s after the first arrival. Some difficulty was initially experienced in deciding whether this was the phase pP or sP. As this radically affects the final best-fitting mechanism and our result for the focal depth differs from previous studies, we examine this question in detail. Interpretation of the strong depth phase as pP is consistent with the 25–30 km depth determined from regional network data. However, the best-fitting mechanism, assuming a 28 km local depth produces synthetic waveforms that do not fit well at three stations (GSC, PAS and TAU). Relatively good fits to the data from all stations were achieved if synthetics were made with an 18 km focal depth, which implies that the prominent depth phase is sP, not pP. The synthetics for each depth for two of the sensitive stations, GSC

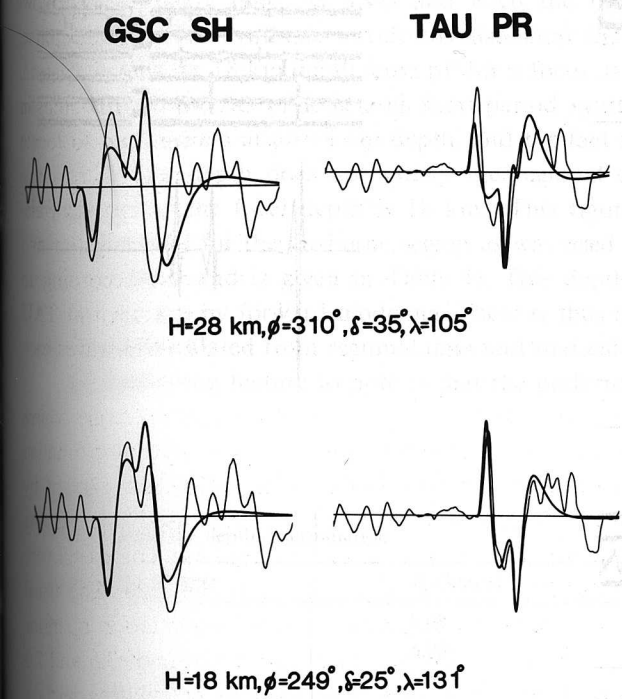

Fig. 3. Data (thin lines) and synthetics (thick lines) for the two best-fitting mechanisms at focal depths of 18 and 28 km for SH and P waveforms at GSC and TAU, respectively.

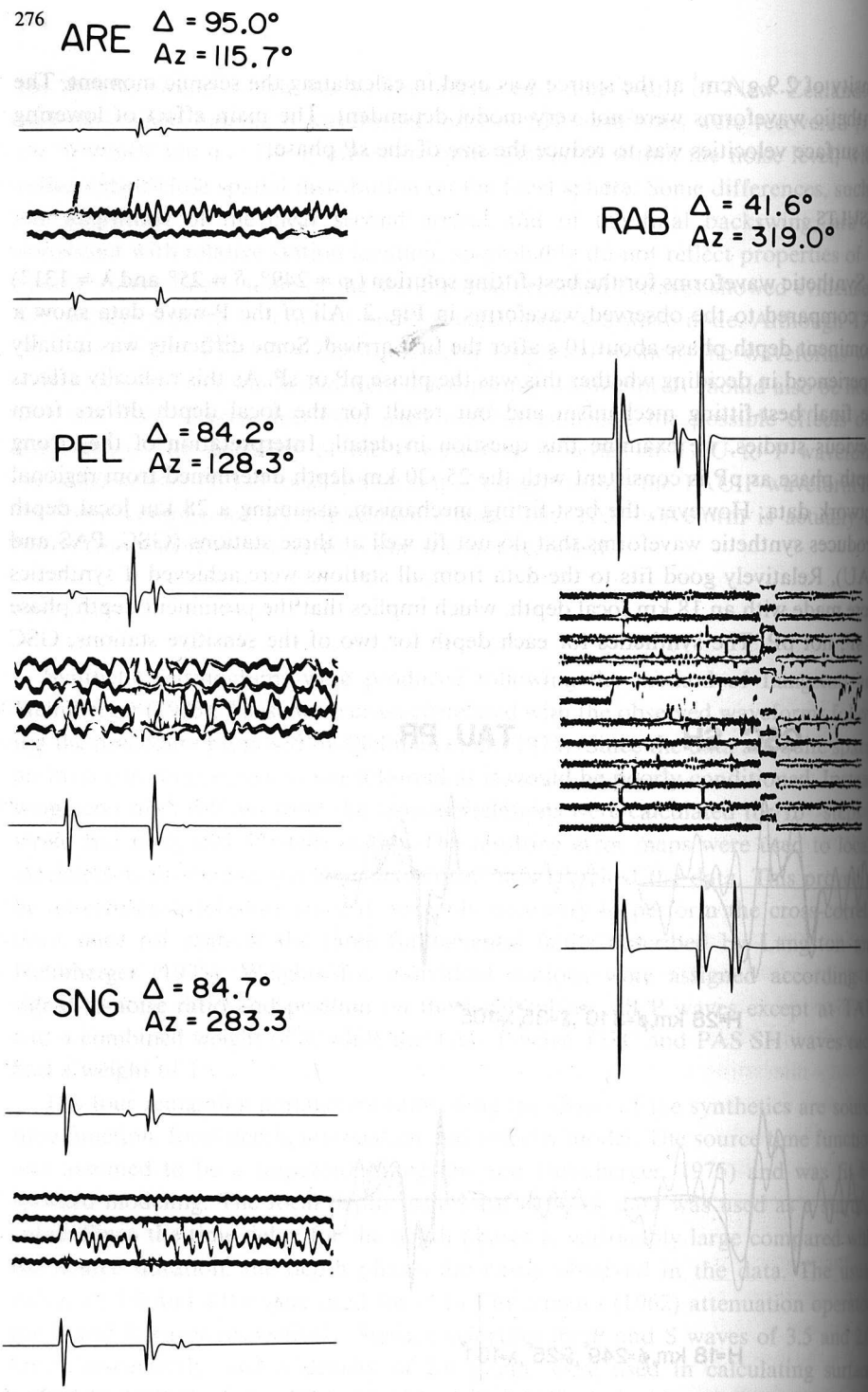

Fig. 4. Short-period vertical waveforms (center traces) recorded at two South American stations ARE and PEL, and two stations at the opposite azimuth RAB and SNG. The top traces are short-period synthetics produced for a mechanism with $\varphi = 249°$, $\delta = 25°$, $\lambda = 131°$ and $H = 18$ km, while the bottom traces are for $\varphi = 310°$, $\delta = 35°$, $\lambda = 105°$ and $H = 28$ km.

and TAU, are shown in Fig. 3. The synthetic SH pulse width for an assumed focal depth of 28 km is wider than that observed at GSC, whereas a good match is obtained when an 18 km depth is used. Since the width of the SH waveform is governed by the S–sS time delay, this provides an unambiguous constraint on the depth. In addition, the choice of an 18 km focal depth provides a superior fit to the TAU waveform compared to that for the 28 km depth. At the greater depth there is a strong trade-off between the TAU P and GSC SH waves becoming nodal.

Further evidence for identifying the prominent depth phase as sP was found by comparing short-period records from the South American stations ARE and PEL, for which there are no long-period data, with short-period records from two stations at opposite azimuths – RAB and SNG. The vertical component waveforms are shown in Fig. 4 along with short-period synthetic seismograms for the best-fitting mechanisms at depths of 18 km ($\varphi = 249°$, $\delta = 25°$ and $\lambda = 131°$) and 28 km ($\varphi = 310°$, $\delta = 35°$ and $\lambda = 105°$). We did not attempt to match the data closely with the synthetics, but instead examined the two most obvious features in the waveforms —the relative amplitudes of initial phases and depth phases, and the time delay until the arrival of a prominent depth phase. Using these criteria, superior fits were obtained for synthetics generated with the best-fitting mechanism for an 18 km focal depth at ARE and PEL, because they correctly reproduced the nodal first arrival and P–sP delay time. At SNG and RAB the fits were equally good for either mechanism. The synthetic waveforms also show the difficulty in distinguishing the phase sP for an 18 km depth from pP for a focus at 28 km.

The superior fits of long and short-period synthetics to the data for the best fitting mechanism at an 18 km depth, and the fact that the best-fitting mechanism for a 28 km depth does not satisfy the regional short-period first motion data, suggests that the focal depth is 18 km. (This figure was obtained with the same velocity model for the Gisborne region as was used for the depth determined from regional data, and is given in Table 1). This depth was found to be constrained within ± 1 km by forward modeling. There is thus a significant difference between the depth calculated from regional data and that calculated from teleseismic data.

An interesting feature to note is that the preferred mechanism also explains the

TABLE 1

Velocity model for depth determination

Depth to top of layer	V_p (km/s)	V_s (km/s)
0	3.00	1.73
2	6.00	3.47
30	6.50	3.70
36	8.10	4.60
41	8.60	4.90

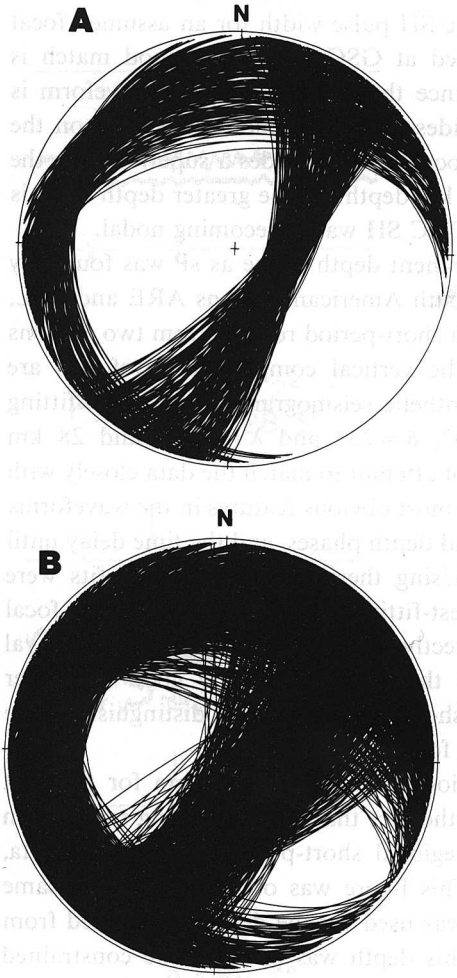

Fig. 5. Possible range of mechanisms for the body-wave solution (A) and for short-period first motion data (B) on equal-area lower hemisphere projections.

absence of recorded SH waveforms at western azimuths – these lie on a P-wave maximum and near a S-wave node, and would have helped constrain the mechanism greatly.

The scalar moment, determined by matching the synthetic and recorded waveform amplitudes was 4×10^{24} dyne-cm. Individual station values ranged from 1.4 to 11.7×10^{24} dyne-cm, with the highest value from the SH waveform at GSC. Rejecting this value gives a mean of 2.8×10^{24} dyne-cm.

A trapeziodal time function of 0.7, 1.0 and 0.7 s was used for the synthetics. Other shapes could fit equally well, but the overall source duration was determined

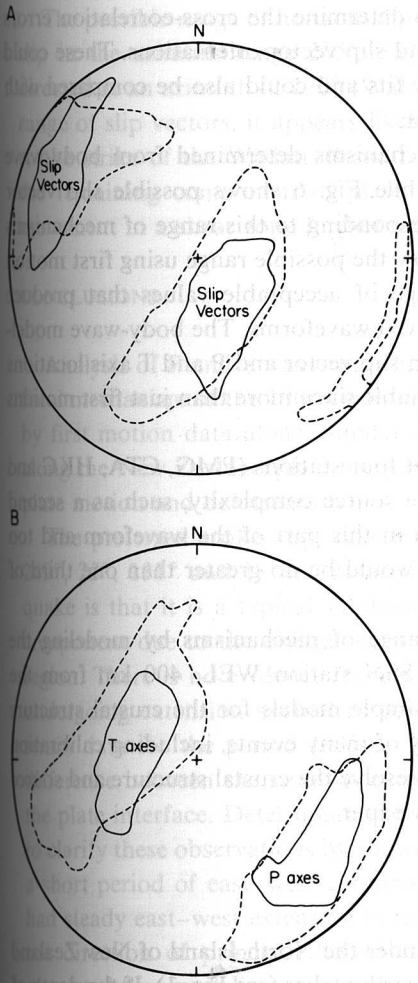

Fig. 6. Contours of possible slip vector orientations (A) and P and T axis locations (B) for the body wave data (solid lines) and short-period first motion data (dashed lines). Projections are as in Fig. 5.

to be in the range 2–3 s. This is within the range of source durations (for an event of this size) for the group of plate boundary events compiled by Liu and Kanamori (1980). Assuming a circular fault, rays leaving at 45° to the normal to the fault plane and, using the formula derived by Geller (1976) and Ebel et al. (1978), we calculated a fault radius of 2.6 to 4.0 km. The stress-drop, calculated from Brune's (1970) circular fault model, is then 20–120 bar.

The most subjective part in determining the degree of constraint on the final focal mechanism was in assessing for which values of cross-correlation error the synthetic fits became unacceptable. Once this was established by eye, an algorithm based on the program FOCPLT (Whitcomb, 1973), which tests all possible double couple

mechanisms in 3.5 degree steps, was used to determine the cross-correlation errors for all mechanisms, *P* and *T* axis locations and slip vector orientations. These could then be contoured to the level of satisfactory fits and could also be compared with similar plots made using the first motion data.

Figure 5 shows the range of possible mechanisms determined from body-wave modelling (A) and first motion data (B), while Fig. 6 shows possible slip vector orientations and *P* and *T* axis locations corresponding to this range of mechanisms for the event. The dashed curves in Fig. 6 show the possible range using first motion data while the solid curves denote the range of acceptable values that produce satisfactory agreement of synthetic and observed waveforms. The body-wave modeling appears to have reduced the uncertainty in slip vector and P and T axis locations by about a factor of two, and is also more reliable since more than just first motions are being matched.

The failure to match the final backswing at four stations (PMG, CTA, HKC and SNG) with the synthetics could suggest some source complexity, such as a second event. However the data are too inconsistent in this part of the waveform and too noisy for this to be modeled. Any sub-event would be no greater than one third of the size of the main event.

It was hoped to further constrain this range of mechanisms by modeling the regional P_{nl} waveform recorded at the WWSSN station WEL, 400 km from the epicenter. This could not be achieved with simple models for the crustal structure between source and receiver. A detailed study of many events, including calibration events with known mechanisms, is needed to resolve the crustal structure and source mechanisms. This is beyond the scope of this paper.

RELATIONSHIP TO REGIONAL TECTONICS

The strike of the subducted Pacific plate under the North Island of New Zealand can be inferred from the distribution of deep earthquakes (see Fig. 1). If the depth of the top surface of the subducted plate inferred by Reyners (1980) (along line *A–A′* in Fig. 1) is the same along its strike, the depth beneath the Gisborne epicenter should be 25 km. The event studied here may thus have occurred just above the plate interface, although it is possible that the subducted plate is shallower in the Gisborne region.

Litte data are available to decide which of the nodal planes is the fault plane. The strike of the plate interface is consistent with that of either nodal plane from our range of mechanisms (Fig. 5), although its dip is consistent with the plane dipping to the northwest (see the dashed curve in Fig. 2). Relocated aftershocks have similar depths to the mainshocks (E.G.C. Smith, pers. commun., 1984), which supports the choice of a shallow-dipping fault plane parallel to the plate interface. A likely mechanism is thus predominantly thrust faulting on a fault plane dipping shallowly to the northwest, with a small right-lateral component.

The possible range of horizontal projections of slip vectors for our solution favour slip in the azimuth range 265°–335°. The relative plate motion in this region is directed at an azimuth of 270° (Walcott, 1978). Since this is near one extreme of the range of slip vectors, it appears likely that slip occurred more nearly perpendicular to the strike of the Wadati–Benioff zone than the plate motion direction and that the remaining component of plate motion is being accommodated by strike-slip movement in a shear zone further inland, as proposed by Walcott (1978).

CONCLUSIONS

Analysis of P and S waveforms has allowed us to provide more constraint on the focal mechanism of the 1966 Gisborne earthquake than has previously been afforded by first motion data alone. Similar analysis of other moderately sized earthquakes along the New Zealand plate boundary may help to refine and constrain models of plate motion and deformation.

The preferred strike, dip, rake and depth of the 1966 Gisborne earthquake are 249°, 25°, 131° and 18 km, respectively. The simplest interpretation of this earthquake is that it is a typical subduction zone thrust event with a small right-lateral component due to the oblique convergence of the Pacific and Indian plates in this region. There is no evidence from our study to suggest that this region is currently undergoing extension normal to the strike of the subducted plate as suggested by strain data for the period 1931 to 1970 (Walcott, 1978), although there may be a difference between the strain occurring in the upper crust and that occurring near the plate interface. Determination of other reliable earthquake mchanisms can help to clarify these observations by showing whether the Gisborne event occurred during a short period of east–west compression in a region that has apparently otherwise had steady east–west extension in the past 50 years, or whether there is a change in the direction of principal horizontal compression with depth in the crust. It is suggested that modeling of teleseismic and regional P and S waveforms may help to provide this data. In particular, the short-period synthetics generated for the best-fitting mechanism for this event can be used as calibration waveforms in modeling smaller events that have occurred in this region.

ACKNOWLEDGEMENTS

Cindy Arvesen, Gladys Engen, Victoria Le Fevre, Art Frankel and Terry Wallace all provided assistance in the initial stages of this work. Martin Reyners and Euan Smith provided us with regional data, and Art Frankel and Hiroo Kanamori made helpful comments on the manuscript. This study was made while one author (THW) was on a Study Award from the Department of Scientific and Industrial Research, New Zealand at the California Institute of Technology, Pasadena. The research was partly supported by the Advanced Research Projects Agency of the Department of

Defence and was monitored by the Air Force Office of Scientific Research under contract number F49620-83-C-0025. Contribution 4133, Division of Geological and Planetary Sciences, California Institute of Technology.

REFERENCES

Adams, R.D. and Ware, D.E., 1977. Subcrustal earthquakes beneath New Zealand; locations determined with a laterally inhomogeneous velocity model. N.Z. J. Geol. Geophys., 20: 59–83.

Brune, J.N., 1970. Tectonic stress and the spectra of seismic shear waves from earthquakes. J. Geophys. Res., 75: 4997–5009.

Ebel, J.E., Burdick, L.J. and Stewart, G.S., 1978. The source mechanism of the August 7, 1966 El Golfo earthquake. Bull. Seismol. Soc. Am., 68: 1281–1292.

Futterman, W.I., 1962. Dispersive body waves. J. Geophys. Res., 67: 5279–5291.

Geller, R.J., 1976. Scaling relations for earthquake source parameters and magnitudes. Bull. Seismol. Soc. Am., 66: 1501–1523.

Hamilton, R.M., 1969. Seismological studies of the Gisborne earthquake sequence, 1966, in Gisborne earthquake New Zealand March 1966. Bull. N.Z. Dep. Sci. Ind. Res., 194: 7–23.

Johnson, T. and Molnar, P., 1972. Focal mechanisms and plate tectonics of the Southwest Pacific. J. Geophys. Res., 77: 5000–5032.

Langston, C.A. and Helmberger, D.V., 1975. A procedure for modelling shallow dislocation sources. Geophys. J.R. Astron. Soc., 42: 117–130.

Liu, H.L. and Kanamori, H., 1980. Determination of source parameters of mid-plate earthquakes from the waveforms of body waves. Bull. Seismol. Soc. Am., 70: 1989–2004.

Mellman, G.R., Burdick, L.J. and Helmberger, D.V., 1975. Determination of source parameters from body wave seismograms. Earthquake Notes, 40: 44.

Reyners, M., 1980. A microearthquake study of the plate boundary, North Island, New Zealand. Geophys. J.R. Astron. Soc., 63: 1–22.

Walcott, R.I., 1978. Geodetic strains and large earthquakes in the axial tectonic belt of North Island, New Zealand. J. Geophys. Res., 83: 4419–4429.

Whitcomb, J.H., 1973. The 1971 San Fernando Earthquake series focal mechanisms and tectonics. Ph.D. Thesis (Part II), California Institute of Technology, Pasadena, Calif.